

SPECTROSCOPIC CONFIRMATION AND VELOCITY DISPERSIONS FOR TWENTY *PLANCK* GALAXY CLUSTERS AT $0.16 < Z < 0.78$

STEFANIA AMODEO¹, SIMONA MEI^{1,2,3,4}, SPENCER A. STANFORD⁵, CHARLES R. LAWRENCE³, JAMES G. BARTLETT^{3,6}, DANIEL STERN³, RANGA-RAM CHARY⁸, HYUNJIN SHIM⁹, FRANCINE R. MARLEAU^{10,7}, JEAN-BAPTISTE MELIN¹¹, CARMEN RODRÍGUEZ-GONZÁLVEZ⁸

¹LERMA, Observatoire de Paris, PSL Research University, CNRS, Sorbonne Universités, UPMC Univ. Paris 06, F-75014 Paris, France

²Université Paris Denis Diderot, Université Paris Sorbonne Cité, 75205 Paris Cedex 13, France

³Jet Propulsion Laboratory, California Institute of Technology, 4800 Oak Grove Drive, Pasadena, California 91011, USA

⁴Cahill Center for Astronomy & Astrophysics, California Institute of Technology, Pasadena, CA 91125, USA

⁵Department of Physics, University of California Davis, One Shields Avenue, Davis, CA 95616, USA ; Institute of Geophysics and Planetary Physics, Lawrence Livermore National Laboratory, Livermore, CA 94550, USA

⁶APC, AstroParticule et Cosmologie, Université Paris Diderot, CNRS/IN2P3, CEA/Irfu, Observatoire de Paris, Sorbonne Paris Cité, 10 rue Alice Domon et Léonie Duquet, 75205, Paris Cedex 13, France

⁷National Optical Astronomy Observatory, Tucson, AZ 85719, USA

⁸Infrared Processing and Analysis Center, California Institute of Technology, Pasadena, CA 91125, USA

⁹Department of Earth Science Education, Kyungpook National University, Republic of Korea

¹⁰Institute of Astro and Particle Physics, University of Innsbruck, 6020, Innsbruck, Austria

¹¹IRFU, CEA, Université Paris-Saclay, F-91191 Gif-sur-Yvette, France

ABSTRACT

We present Gemini and Keck spectroscopic redshifts and velocity dispersions for twenty clusters detected via the Sunyaev-Zel'dovich (SZ) effect by the *Planck* space mission, with estimated masses in the range $2.3 \times 10^{14} M_{\odot} < M_{500}^{\text{Pl}} < 9.4 \times 10^{14} M_{\odot}$. Cluster members were selected for spectroscopic follow-up with Palomar, Gemini and Keck optical and (in some cases) infrared imaging. Seven cluster redshifts were measured for the first time with this observing campaign, including one of the most distant *Planck* clusters confirmed to date, at $z = 0.782 \pm 0.010$, PSZ2 G085.95+25.23. The spectroscopic redshift catalogs of members of each confirmed cluster are included as on-line tables. We show the galaxy redshift distributions and measure the cluster velocity dispersions. The cluster velocity dispersions obtained in this paper were used in a companion paper to measure the *Planck* mass bias and to constrain the cluster velocity bias.

Keywords: cosmology:observations — galaxies: clusters: general — galaxies: distances and redshifts

1. INTRODUCTION

Massive galaxy clusters are sensitive cosmological probes (e.g. [Allen et al. 2011](#)), yet these are rare objects best found in all-sky surveys covering large volumes. The *ROSAT* All-Sky Survey (RASS, [Truemper 1993](#)) dates back to the early 1990s and has served the community as a workhorse since, providing hundreds of cluster candidates. A subsequent important step has been taken by the *Planck* satellite, launched on 2009 May 14. *Planck* detects clusters based on the Sunyaev-Zel'dovich (SZ) effect ([Sunyaev & Zeldovich 1970](#); [Birkinshaw 1999](#); [Carlstrom et al. 2002](#)), i.e. the distortion of the energy spectrum of cosmic microwave background (CMB) photons passing through the cluster due to inverse Compton scattering with hot electrons. Being independent of distance, the SZ signal does not suffer from cosmological dimming and it is proportional to the cluster mass. Benefiting from this, *Planck* extends the (X-ray) RASS catalog to higher red-

shift and contains a large fraction of massive objects of the type most prized for cosmological studies.

Planck has produced two all-sky cluster surveys through the SZ effect ([Planck Collaboration et al. 2014, 2016b](#)): the PSZ1 with 1227 candidates based on 15.5 months of data, and the PSZ2 with 1653 candidates from the full mission dataset of 29 months. Of the PSZ2 candidates, 1203 have been confirmed by ancillary data and 1094 have redshift estimates, in the range $0 < z < 1$, with a mean redshift of $z \sim 0.25$. The mean mass of the confirmed clusters over the whole redshift range is $M_{500}^{\text{Pl}} = 4.82 \times 10^{14} M_{\odot}$ (see the definition of M_{500}^{Pl} below).

The *Planck* collaboration has undertaken a large follow-up effort to confirm cluster candidates and measure their redshifts. The first optical follow-up was based on observations with the Russian-Turkish 1.5 m telescope ([Planck Collaboration et al. 2015](#)) and provided spectroscopic redshifts of 65

Planck clusters. The second optical follow-up, based on observations with telescopes at the Canary Islands Observatories, yielded 53 cluster spectroscopic redshifts (Planck Collaboration et al. 2016c). The *Planck* collaboration has also carried out X-ray validation programs with *XMM-Newton* (Planck Collaboration et al. 2011a, 2012, 2013), where redshifts for 51 clusters were obtained from X-ray spectral fitting.

Our follow-up program presented in this paper includes the spectroscopic follow-up of 20 *Planck* cluster candidates with the Gemini and Keck telescopes (P.I. J.G. Bartlett and F.A. Harrison, respectively). The goals of our programs were: (1) to confirm *Planck* SZ detections as clusters and measure their redshifts; (2) to estimate their masses using cluster galaxy velocity dispersions; and (3) to measure the *Planck* mass and velocity bias. We use SDSS (Sloan Digital Sky Survey; York et al. 2000), and Palomar and Gemini imaging to select the cluster galaxies to target with spectroscopy.

In this paper, we describe our observations and publish the optical spectroscopy of cluster members, from which we derive the cluster redshifts and velocity dispersions. In a companion paper (Amodeo et al. 2017), we use these observations to estimate the clusters’ dynamical masses and calibrate the all-important relation between the SZ Compton parameter, Y , and mass.

The paper is organized as follows. In Section 2 we present our sample of *Planck*-selected clusters and describe the observing programs carried out at the Palomar, Gemini and Keck telescopes. A table describing all the targets observed with the Palomar telescope is given in Appendix A. In Section 3 we describe the spectroscopic redshift and galaxy velocity dispersion measurements. For clusters with a spectroscopic follow-up, we include figures of redshift histograms, optical images and SZ maps in Appendix B. Catalogs of cluster member galaxies with spectroscopic measurements are included as on-line tables. We illustrate the parameters published in the catalogs in Section 4 and give an example in Appendix C. In Section 5 we discuss our results in the context of optical identifications of *Planck* clusters.

Throughout this paper, masses are quoted at a radius R_Δ , within which the cluster density is Δ times the critical density of the universe at the cluster’s redshift, where $\Delta = \{200, 500\}$. We refer to the $\Delta = 200$ radius as the “virial radius”, R_{200} . Mass and radius are directly connected via $M_\Delta \equiv \Delta H_z^2 R_\Delta^3 / (2G)$, where H_z is the Hubble constant at the cluster’s redshift.

2. DATA AND OBSERVATIONS

In this section we describe our spectroscopic observations with the Gemini and Keck telescopes, and the Palomar telescope imaging that was used to select cluster members. The details of each observing run (pre-imaging and optical spectroscopy) are listed in Table 1.

Since it is well-known that early-type galaxies (ETGs) in

clusters define a tight red-sequence up to redshift $z \sim 1.5$ (Mei et al. 2009), and can be easily identified with respect to field background galaxies, we selected cluster members to follow-up with spectroscopy from optical and infrared imaging using a red sequence search method (Gladders & Yee 2000; Licitra et al. 2016a,b). For most clusters, we used g' and i' filters for imaging, since the ETG ($g - i$) color is monotonic over the redshift range in which most of *Planck* clusters are detected, $z < 1$. We also observed the r' band, when possible within our exposure time constraints, to obtain better photometric redshifts. For the candidates that appeared to be at $z > 0.6$ from their *WISE* imaging in the mid-infrared (see the *WISE* analysis in Planck Collaboration et al. 2016b), we obtained near-infrared observations in the J and K bandpasses. For some of our targets, we could not obtain images at two different wavelengths and used SDSS photometry when available.

Cluster members were selected as red sequence galaxies by their colors, using Bruzual & Charlot (2003) stellar population models and Mei et al. (2009) empirical red sequence measurements, following the cluster member selection technique described in Licitra et al. (2016a,b), adapted for the bandpasses available for these observations.

2.1. Gemini Observations

The Gemini imaging and spectroscopic follow-up was performed with GMOS-N and GMOS-S at the Gemini-North and Gemini-South Telescopes, respectively, in the programs GN-2011A-Q-119, GN-2011B-Q-41, and GS-2012A-Q-77 (P.I. J.G. Bartlett). This sample consists of 19 *Planck*-detected galaxy clusters, 17 of which are part of the *Planck* PSZ2 catalog (Planck Collaboration et al. 2016b), and one is published in the *XMM-Newton* validation follow-up of *Planck* cluster candidates (Planck Collaboration et al. 2013). Two clusters are not part of the already published *Planck* papers: (1) PLCK G183.33-36.69 has a detection signal-to-noise ratio (S/N) just below the *Planck* catalog selection threshold and (2) PLCK G147.32-16.59 is in the *Planck* cluster mask.

The goal of our Gemini program was to obtain a statistical calibration of the *Planck* SZ mass estimator. For this purpose, we mostly chose clusters that were detected with a *Planck* SZ S/N of about 4.5σ or larger, distributed in the Northern and Southern Hemispheres, spanning a wide range in *Planck* SZ masses, $2 \times 10^{14} M_\odot \lesssim M_{500}^{\text{Pl}} \lesssim 10^{15} M_\odot$, in the redshift range $0.16 < z < 0.44$. In Figure 1, we compare our sample to the full PSZ2 catalog. These histograms show that our selection has an average redshift larger than the PSZ2 catalog, and a mass range covering most of the mass range of the PSZ2 catalog. In fact, our sample has an average redshift of $z = 0.37$ and an average mass of $M = 6.2 \times 10^{14} M_\odot$, compared to the average PSZ2 redshift and mass of $z = 0.25$ and $4.8 \times 10^{14} M_\odot$, respectively. The larger average redshift was chosen to cover most of the cluster members within $\sim R_{200}$

Table 1. Observation details.

Run	Semester	PI	Tel./Inst.	Program ID	N_{cl}
1	2010B	Lawrence	Palomar/LFC,WIRC		11
2	2011A	Lawrence	Palomar/LFC		25
3	2011B	Lawrence	Palomar/LFC		15
2	2011A	Bartlett	Gemini-N/GMOS	GN-2011A-Q-119	11
3	2011B	Bartlett	Gemini-N/GMOS	GN-2011B-Q-41	11
4	2012B	Lawrence	Palomar/LFC		9
5	2012A	Bartlett	Gemini-S/GMOS	GS-2012A-Q-77	9
6	2013B	Harrison	Keck/LRIS	UT 2013 October 4-5	1

in the field of view of the Gemini and Keck telescopes.

The Northern sample was selected in the area covered by the SDSS, and we used the SDSS public releases and our GMOS-N pre-imaging in the r -band (150 s) to detect red galaxy over-densities around the *Planck* detection center. When unknown, we estimated the approximate cluster redshift using its red sequence to calculate the appropriate exposure times for the spectroscopic follow-up. For PSZ2 G139.62+24.18, PSZ2 G157.43+30.34 and PLCK G183.33-36.69, we used imaging obtained with the Palomar telescope. For the Southern sample, we obtained GMOS-S pre-imaging in the g and i -bands (200 s and 90 s integrations, respectively).

Our GMOS spectroscopic observations were reduced using the IRAF Gemini GMOS package and standard techniques. After co-adding the reduced exposures, we extracted one-dimensional spectra for the objects in each slitlet and initially inspected them visually to identify optical features such as the 4000 Å break, G-band, Ca H+K absorption lines, and, rarely, [O II]λ3727 emission. We determined more precise galaxy redshifts by running the IRAF task *xcsao*. In Figure 2, we show two Gemini/GMOS spectra of galaxies in the cluster PSZ2 G250.04+24.14.

The clusters that we followed-up with the Gemini telescopes are listed in Table 2 (see also Table 1 from [Amodeo et al. 2017](#)). The mass calibration derived from the velocity dispersions of the clusters in this sample is discussed in [Amodeo et al. \(2017\)](#), in which we measured the *Planck* mass bias and constrained the cluster velocity bias.

2.2. Keck Observations

We obtained spectroscopy of PSZ2 G085.95+25.23 on the nights of UT 2013 October 4-5 using the dual-beam Low Resolution Imaging Spectrometer (LRIS; [Oke et al. 1995](#)) on the Keck I telescope atop Mauna Kea. These slitmask observations were obtained with the 400 ℓ mm⁻¹ grism on the blue arm of LRIS ($\lambda_{\text{blaze}} = 3400$ Å), the 400 ℓ mm⁻¹ grating on the red arm of LRIS ($\lambda_{\text{blaze}} = 8500$ Å), and the 5600 Å dichroic was used to split the light. We obtained three 1200 s

integrations on the first night through variable cloud cover, and two 1200 s integrations on the second night in photometric conditions. After some experimentation, we base our analysis on the single best exposure from the first night combined with the two exposures from the second night. The data were processed using standard techniques within IRAF, and flux calibrated using standard stars from [Massey & Gronwall \(1990\)](#) observed on the second night.

In Figure 3, we show two Keck/LRIS spectra of galaxies in the cluster PSZ2 G085.95+25.23.

2.3. Palomar Optical and Infrared Imaging

The Palomar optical and infrared imaging, used to select cluster members, was obtained with a dedicated *Planck* follow-up program (PI: C. Lawrence) that included several runs. Our Palomar sample is presented in the Appendix, in Table A1.

For the Palomar/WIRC data reduction, we pre-processed the images using a dedicated IRAF package `noao.imred.ccdred`. Master dark frames of different exposure times were constructed for each night of observation, and these were subtracted from science images of the corresponding exposure time. Dark-subtracted individual science images were then divided by the master flat image in the same filter. We tested two ways of constructing the master flat image: first, by combining dome flats after the dark correction (master domeflat) and, second, by median combining all science images (master skyflat). Since there was little difference between the two master flat images, we chose to use the master domeflat in the flat correction. Sky subtraction, bad pixel and cosmic ray masking, image aligning and combining were done using the IRAF package `xdimsum`¹. Bad pixel masks were created from the master skyflat image by identifying bad, hot, or warm pixels significantly ($> 20\sigma$) lower or higher than the average background. After calculating the shifting of the images that

¹ Experimental Deep Infrared Mosaicing Software

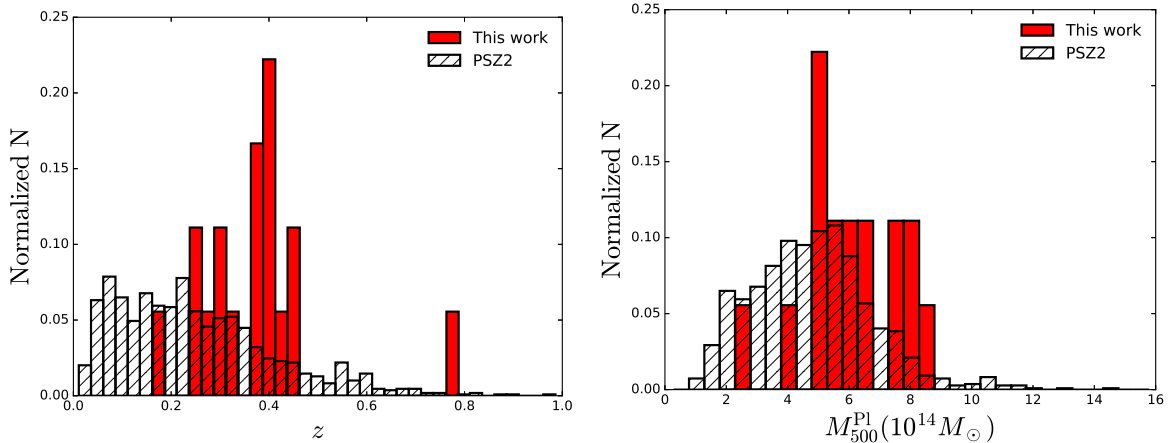


Figure 1. Histograms of the redshifts (left) and the masses (right) of our spectroscopic sample compared to the full PSZ2 catalog. These histograms are normalized to the total number of objects in each sample. We have selected cluster candidates with redshift $z > 0.2$ (with average redshift larger than the PSZ2 catalog), and larger average mass than the PSZ2 catalog, with cluster masses in the range $2.3 \times 10^{14} M_{\odot} < M_{500}^{\text{Pl}} < 9.4 \times 10^{14} M_{\odot}$. The cluster mass shown here is the *Planck* mass proxy (Planck Collaboration et al. 2016b).

were to be sky subtracted, we performed the sky subtraction correcting for bad pixels and cosmic rays. The six adjacent images were used to calculate the sky. Once the mosaic image was created, we created an object mask from the mosaic image, repeated the sky subtraction and combining process to obtain the final mosaic image as well as the exposure time map. Astrometric calibration was done using the 2MASS point source catalog as a reference through the IRAF package `ccmap`.

The optical Palomar/LFC data reduction comprised basic pre-processing (i.e., bias, dark, flat, crosstalk and overscan/trim correction), satellite trail removal, bad pixel and cosmic ray correction, and aligning and co-adding individual images to produce the final mosaic images. Since the LFC data were stored in a multi-extension fits (MEF) format, we mostly used the IRAF package `mscred` (Valdes et al. 1995) as well as `ccdred` for the analysis. The initial bad pixel masks were generated from the ratio between two flat-field images with different exposure times. After the bias, dark, flat, crosstalk and overscan correction using `ccdproc`, satellite trails in each image were identified using the IRAF task `satzap` and corrected. In addition, initial bad pixels and cosmic rays were identified using average sigma clipping. The updated bad pixel masks were converted to weight images used later in the coadding step.

Fringe correction was necessary for images taken with the i' -band filter. The fringe effect is less noticeable in images with short exposure times (< 300 s), but the interference pattern significantly affects the background for longer exposures. For fringe correction, we first made an object mask and the resulting sky map for each image using the IRAF `nproto.objmasks`. Then the output sky maps were combined using `mscred.sflatcombine` to produce the response sky image, from which the median-filtered response

was subtracted to derive the fringe pattern. Using the fringe pattern as the input in `mscred.rmfringe`, the fringes in i' -band images were successfully divided out. After these corrections, astrometric calibration was done with `ccmap` using the USNO-B1.0 catalog as a reference. Then the images for each target were registered and mosaicked using the Terapix/*Swarp* software. The images were background subtracted, resampled, and combined to produce weighted means of the individual images for flux conservation. The weight images previously created from the final bad pixel masks were used.

Many of our Palomar nights were not photometric, and we could not obtain accurate photometric redshifts with only a few bandpasses. However, we could use SDSS and our Palomar images to select cluster member candidates for our Gemini spectroscopic observations.

3. CLUSTER CONFIRMATION AND SPECTROSCOPIC REDSHIFT MEASUREMENTS

We calculated the cluster redshifts and velocity dispersions using the ROSTAT software (Beers et al. 1990) with the bi-weight method (see Table 3). This is appropriate to our clusters where there are typically 20 confirmed members. We also report the dispersion σ_G determined from the gapper estimator (as implemented in ROSTAT), which is to be preferred for clusters with fewer than 10-15 members (see Giardi et al. 1993, 2005). We find that biweight and gapper estimates are perfectly consistent, with the absolute difference between the velocity dispersions calculated from the two methods being on average of (0.04 ± 0.14) sigma, and never higher than 0.5 sigma. Since the line-of-sight cluster velocity dispersion can be highly anisotropic, small galaxy samples lead to large systematic uncertainties, with estimated uncertainties of $\lesssim 10\%$ (White et al. 2010) for samples with more than ~ 10 -15 galaxies like ours.

Table 2. Spectroscopically confirmed cluster sample. Clusters are named after their PSZ2 ID, when available. When it is not available, we use the prefix ‘PLCK’ followed by a notation in Galactic coordinates similar to that used in the PSZ2 paper. Right ascension and declination indicate the optical cluster centre. Filter names used for imaging, spectroscopic observing times and the number of masks are also stated. The last column lists the observing run(s) for each target, including pre-imaging.

Name	R.A. (deg)	Decl. (deg)	Filter	t_{exp} (s)	N_{mask}	Run
PSZ2 G033.83-46.57	326.3015	-18.7159	<i>g,i</i>	1800	2	GS-2012A-Q-77
PSZ2 G053.44-36.25	323.8006	-1.0493	<i>r</i>	1800	1	GN-2011A-Q-119,GN-2011B-Q-41
PSZ2 G056.93-55.08	340.8359	-9.5890	<i>r</i>	1800	2	GN-2011A-Q-119,GN-2011B-Q-41
PSZ2 G081.00-50.93	347.9013	3.6439	<i>r</i>	1800	1	GN-2011A-Q-119,GN-2011B-Q-41
PSZ2 G083.29-31.03	337.1406	20.6211	<i>r</i>	1800	1	GN-2011A-Q-119,GN-2011B-Q-41
PSZ2 G085.95+25.33	277.6164	56.8823	–	3600	2	Keck Telescope
PSZ2 G108.71-47.75	3.0715	14.0191	<i>r</i>	1800	2	GN-2011A-Q-119,GN-2011B-Q-41
PSZ2 G139.62+24.18 ^a	95.4529	74.7014	<i>r</i>	900	2	GN-2011A-Q-119,GN-2011B-Q-41
PLCK G147.32-16.59 ^b	44.1101	40.2853	<i>r</i>	1800	2	GN-2011A-Q-119,GN-2011B-Q-41
PSZ2 G157.43+30.34 ^a	117.2243	59.6974	<i>r</i>	3600	2	GN-2011A-Q-119,GN-2011B-Q-41
PLCK G183.33-36.69 ^a	57.2461	4.5872	<i>r</i>	1800	2	GN-2011A-Q-119,GN-2011B-Q-41
PSZ2 G186.99+38.65	132.5314	36.0717	<i>r</i>	1800	2	GN-2011A-Q-119,GN-2011B-Q-41
PSZ2 G216.62+47.00	147.4658	17.1196	<i>r</i>	1800	2	GN-2011A-Q-119,GN-2011B-Q-41
PSZ2 G235.56+23.29	134.0251	-7.7207	<i>g,i</i>	900	2	GS-2012A-Q-77
PSZ2 G250.04+24.14	143.0626	-17.6481	<i>g,i</i>	1800	2	GS-2012A-Q-77
PSZ2 G251.13-78.15	24.0779	-34.0014	<i>g,i</i>	900	2	GS-2012A-Q-77
PSZ2 G272.85+48.79	173.2938	-9.4812	<i>g,i</i>	900	2	GS-2012A-Q-77
PSZ2 G329.48-22.67	278.2527	-65.5555	<i>g,i</i>	900	2	GS-2012A-Q-77
PSZ2 G348.43-25.50	291.2293	-49.4483	<i>g,i</i>	900	2	GS-2012A-Q-77
PSZ2 G352.05-24.01	290.2320	-45.8430	<i>g,i</i>	1200	2	GS-2012A-Q-77

^aAlso observed at Palomar, see Table A1.

^bTarget PLCK G147.32-16.59 is confirmed in the *XMM-Newton* cluster validation (Planck Collaboration et al. 2013), but it is not included in the two *Planck* catalogues of SZ sources released so far.

We retain as possible cluster members the galaxies within 3σ of the average cluster velocity/redshift. Standard deviations are in the range 0.001-0.008 in redshift, for the clusters that we confirm, apart PLCK G147.32-16.59 that shows evidence for an undergoing merger event (see discussion below). Figures B1 and B2 show the redshift distributions of the cluster member galaxies (left), the optical image of the cluster with the selected members (middle), and the SZ maps in units of S/N (right), for the Northern and the Southern samples, respectively. We also present Gaussian fits to the redshift distributions in the left-hand panels.

The middle panels of Figures B1 and B2 show the optical pre-imaging, within the Gemini field of view of 5.5×5.5 arcmin². Spectroscopically confirmed members are indicated by green circles.

For PSZ2 G056.93-55.08 we visually observe three spatially separated galaxy groups, but all at the same redshift

and within one virial radius. We derived the virial radius $R_{200} = (2.00 \pm 0.05)$ Mpc from the SZ mass estimate of $M_{500}^{\text{Pl}} = (9.4 \pm 0.5) \times 10^{14} M_{\odot}$ ². At the cluster redshift, $z = 0.443$, 2 Mpc correspond to 5.7 arcmin in a Planck cosmological model (Planck Collaboration et al. 2016a). We cannot obtain a separate mass estimate for each group because the Planck beam includes all the three groups and we do not have enough spectroscopic members of each group for deriving the group mass from velocity dispersions. Therefore, we consider the three groups as being part of a single cluster detection.

For all targets but PSZ2 G352.05-24.01, the red circled area is centered on the optical center of the cluster and has

² See Appendix A in Amodeo et al. (2017) for the conversion from M_{500}^{Pl} to M_{200}^{Pl} .

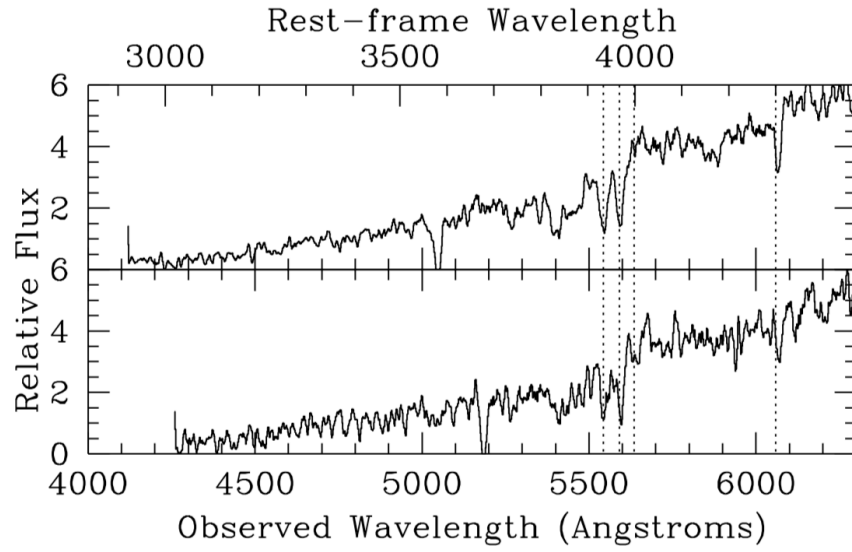


Figure 2. Spectra obtained with Gemini/GMOS for two galaxies in the cluster PSZ2 G250.04+24.14 ($z = 0.411$). The vertical dotted lines represent Ca H+K, D4000, and the G-band, respectively.

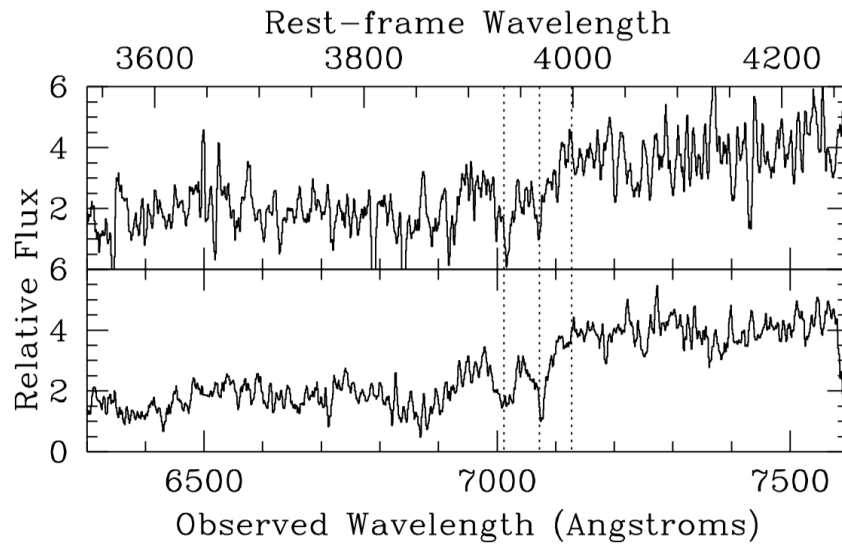


Figure 3. Spectra obtained with Keck/LRIS for two galaxies in the cluster PSZ2 G085.95+25.23 ($z = 0.782$). The vertical dotted lines represent Ca H+K and D4000, respectively.

a 1 arcmin radius. The optical center was obtained as the brightest cluster member in the densest cluster region, following a modified version of the centering algorithm from Licitra et al. (2016a). For PSZ2 G352.05-24.01, we used the coordinates of the X-ray center, marked with a red cross.

In the right-hand panels, we show the SZ maps with the same area enclosed by the black circles and centered on the optical position. The SZ maps have an angular resolution of 5 arcmin and are given in units of S/N . All the detections lie above $S/N = 4.5$, except for PLCK G183.33-36.69 with $S/N = 2$.

Masses and S/N were recalculated from a re-extraction of the SZ signal using the Matched Multi-Filter MMF3 (Melin et al. 2006; Planck Collaboration et al. 2011b, 2014, 2016b), fixing the position to the optical position and varying the filter size. They are reported in Table 3. The quoted S/N is the maximum across the various filter sizes at the optical position. The masses are obtained from the re-extracted SZ signal following the method described in Sec. 7.2.2 of Planck Collaboration et al. (2014).

In Table 3, we also show the number of detection methods from Planck Collaboration et al. (2016b). The Planck selection function is very reliable ($> 90\%$) for detections obtained with $S/N > 4.5$ by at least one detection method. For objects detected with all three detection methods, the probability of being a cluster is $> 98\%$ with $S/N > 4.5$ (Planck Collaboration et al. 2016b). In order to confirm each target as galaxy cluster, we combine this information with the probability that the galaxy redshift distribution is Gaussian, the characteristic distribution of a virialized cluster, from the Kolmogorov-Smirnov (K-S, e.g. Fasano & Franceschini 1987) and the Shapiro-Wilk (S-W, Shapiro & Wilk 1965) statistics, as well as the probability of a uniform distribution from a K-S test. The results of these tests are shown in the last three columns of Table 3.

Eleven of our cluster candidates have $> 98\%$ probability of being a galaxy cluster, since they were detected with three detection methods and have $S/N > 4.5$. For these targets, the probabilities that the redshift distributions are Gaussian are almost always $> 80\%$ and the probabilities to be uniform always $< 50\%$ and mostly $< 10\%$. Only one object, PSZ2 G139.62+24.18 at $z=0.268$, has a $S/N = 9.5$, which corresponds to a *Planck* reliability of being a cluster of $\sim 100\%$, but a K-S (S-W) probability of having a Gaussian redshift distribution of $\sim 50\%$ ($\sim 20\%$), and the probability of having a uniform redshift distribution of $\sim 20\%$. It shows a very luminous BCG at the center, and has 20 spectroscopically confirmed galaxies at the same redshift. All these elements lead us to believe that this is a galaxy cluster, and it was also confirmed as a cluster in the PSZ2 catalog. All the other ten targets are mostly likely galaxy clusters, and we assume that they are. Of those, we confirm three clusters that were not originally confirmed in the PSZ2.

The other cluster candidates that were detected with at least

one detection method and $S/N > 4.5$ have a $> 90\%$ probability of being galaxy clusters. For these candidates, we assume that we confirm a cluster when the probability that their redshift distribution is Gaussian is $> 95\%$ ($\sim 2\sigma$). On the other hand, we do not confirm a cluster when the probability of a uniform distribution is $> 50\%$. In fact, since the *Planck* detection and the galaxy redshift distribution are two independent events, we can multiply the *Planck* probability of not being a cluster ($\sim 10\%$) by the probability of having a uniform distribution of galaxy redshifts. If this last is $< 50\%$, the total probability that the candidate is not a cluster is $< 5\%$. Among these last targets, three have a probability that their redshift distribution is Gaussian is $> 95\%$ ($\sim 2\sigma$), and we consider them as confirmed clusters. All three are new confirmation with respect to PSZ2.

Three of the targets that were only detected by one method, though, and one candidate detected with two methods show less definitive results. We discuss these last cluster candidates in more detail below.

PLCK G147.32-16.59 was detected by one method with a high S/N ($S/N \sim 6$), and its redshift distribution has a probability of $\sim 90\%$ of being Gaussian; however, it also has a $\sim 10\%$ probability of not being a cluster. With only 10 confirmed members, its confirmation is not very reliable, but it is more probable that it is a cluster or a group of galaxies than a uniform redshift distribution, and we consider it a confirmed cluster. *XMM-Newton* observations (Planck Collaboration et al. 2013) reveal two substructures in the X-ray surface brightness, indicating that it is undergoing a merger event (see also van Weeren et al. 2014; Mroczkowski et al. 2015). Because of the undergoing merger, we have excluded this cluster from the analysis of the velocity dispersion–mass relation in Amodeo et al. (2017).

PLCK G183.33-36.69 was detected by one method with a $S/N \sim 2$ (*Planck* reliability of $< 70\%$), its redshift distribution has a K-S (S-W) probability of $\sim 60\%$ ($\sim 5\%$) to be Gaussian, and a $\sim 1\%$ total probability of not being a cluster. However, we can clearly see the two bright central galaxies in the Gemini image, and the cluster center is close to the border of the Gemini field. It seems to us that this cluster was not enough well centered in the Gemini imaging and spectroscopy to obtain a significant sample to confirm it, even if it has a larger probability to be a cluster or group of galaxies instead of an uniform galaxy distribution. The SZ flux gives a mass of $M_{500}^{\text{Pl}} = 2.3_{-0.9}^{+0.7} \times 10^{14} M_{\odot}$, and its galaxy velocity dispersion is $\sigma_{200} = 842_{-451}^{+297} \text{ km s}^{-1}$. We consider it as a confirmed cluster, and warn the reader about the larger uncertainty (with respect to most of the remaining sample) in the velocity dispersion measurement and its redshift distribution skewness, which both might indicate an unrelaxed dynamical state. We kept this cluster in our sample in Amodeo et al. (2017) because, due to the large uncertainty on the velocity dispersion measurement, it does not significantly weight on our final results.

Table 3. Columns from left to right list the cluster ID, our measured spectroscopic redshift, the new spectroscopic redshift estimates, redshift estimates obtained including the available redshifts in the SDSS DR14, the total number of galaxies with measured redshifts in the cluster field, the number of confirmed member galaxies, and our measured velocity dispersions using the biweight and the gapper methods (Beers et al. 1990). The next three columns give, respectively, the signal-to-noise ratio, the number of detection methods and the *Planck* mass proxy, as reported in the PSZ2 catalog (we calculated these numbers for the two objects not listed in the PSZ2 catalog). The last three columns list, respectively, the Kolmogorov-Smirnov (K-S) and the Shapiro-Wilk (S-W) statistics for the probability that the redshift distributions are Gaussian, and the K-S test for a uniform distribution.

Name	z_{spec}	New z_{spec}	$z_{\text{spec+DR14}}$	N_{tot}	$N_{\text{gal}}^{\text{conf}}$ (km/s)	σ_{BI}	$\sigma_{\text{BI+DR14}}$	σ_{G} ($10^{14} M_{\odot}$)	SNR	Det. Meth.	M_{500}^{Pl}	K-S gaussian prob.	S-W gaussian prob.	K-S uniform prob.
PSZ2 G033.83-46.57	0.439 ± 0.001	+		10	8	985 ⁺⁴⁵¹ ₋₂₁₀		1051 ⁺³⁰⁹ ₋₂₁₄	4.6	2	5.4 ^{+0.7} _{-0.8}	0.96	0.71	0.50
PSZ2 G053.44-36.25	0.331 ± 0.001	+	0.3295 ± 0.0003	21	20	1011 ⁺²⁴² ₋₁₃₁	1215 ⁺¹⁶⁷ ₋₁₀₀	1025 ⁺²²⁴ ₋₁₁₇	8.9	3	7.5 ^{+0.5} _{-0.6}	0.99	0.80	0.07
PSZ2 G056.93-55.08	0.443 ± 0.001		0.4430 ± 0.0001	49	46	1356 ⁺¹⁹² ₋₁₂₇	1331 ⁺¹⁸⁴ ₋₁₂₈	1345 ⁺¹⁷⁰ ₋₁₁₃	11.5	3	9.4 ± 0.5	0.76	0.12	0.01
PSZ2 G081.00-50.93	0.303 ± 0.001	+	0.4430 ± 0.0001	15	15	1292 ⁺³⁶⁰ ₋₁₈₅	1552 ⁺¹⁷⁵ ₋₁₅₄	1300 ⁺³²⁶ ₋₁₄₀	9.2	3	6.7 ± 0.5	0.97	0.96	0.14
PSZ2 G083.29-31.03	0.412 ± 0.002		0.4123 ± 0.0001	21	20	1434 ⁺⁵⁷⁴ ₋₃₂₀	1153 ⁺¹¹¹ ₋₉₄	1591 ⁺³⁷⁶ ₋₂₆₂	9.1	3	7.8 ^{+0.5} _{-0.6}	0.83	0.90	0.004
PSZ2 G085.95+25.23	0.782 ± 0.003	+		16	14	1049 ⁺²¹⁰ ₋₁₈₀		1041 ⁺¹⁹⁵ ₋₁₁₉	5.0	2	5.2 ^{+0.6} _{-0.7}	0.91	0.05	0.06
PSZ2 G108.71-47.75	0.389 ± 0.001		0.3897 ± 0.0002	11	8	900 ⁺⁴⁵⁸ ₋₁₉₀	861 ⁺³²⁷ ₋₂₁₆	900 ⁺⁴⁸⁰ ₋₁₈₃	4.3	1	5.1 ^{+0.7} _{-0.9}	0.99	0.87	0.65
PSZ2 G139.62+24.18	0.268 ± 0.001			20	20	1120 ⁺³⁶⁶ ₋₂₃₈		1127 ⁺³⁰⁵ ₋₁₇₁	9.6	3	7.3 ± 0.5	0.51	0.25	0.20
PLCK G147.32-16.59	0.640 ± 0.009			10	10	–		–	5.9	1	8.1 ^{+0.8} _{-0.9}	0.91	0.91	0.86
PSZ2 G157.43+30.34	0.402 ± 0.001	+		28	28	1244 ⁺¹⁹² ₋₁₀₉		1242 ⁺¹⁹⁵ ₋₁₀₃	8.8	2	8.2 ± 0.6	0.99	0.73	0.23
PLCK G183.33-36.69	0.163 ± 0.001			11	11	897 ⁺⁴³⁷ ₋₂₇₅		979 ⁺²⁶³ ₋₁₈₇	2.1	1	2.3 ^{+0.7} _{-0.9}	0.59	0.05	0.04
PSZ2 G186.99+38.65	0.377 ± 0.001		0.3774 ± 0.0003	41	41	1506 ⁺¹⁶⁴ ₋₁₂₀	1426 ⁺¹³³ ₋₈₇	1462 ⁺¹⁶⁵ ₋₁₀₂	7.1	3	6.6 ^{+0.6} _{-0.7}	0.83	0.32	0.40
PSZ2 G216.62+47.00	0.385 ± 0.001		0.3864 ± 0.0003	37	37	1546 ⁺¹⁷⁴ ₋₁₂₂	1779 ⁺²⁰⁷ ₋₁₅₃	1524 ⁺¹⁷⁸ ₋₁₁₀	9.7	3	8.4 ^{+0.5} _{-0.6}	0.97	0.45	0.86
PSZ2 G235.56+23.29	0.375 ± 0.002			27	23	1644 ⁺²⁸⁵ ₋₁₉₂		1636 ⁺²⁹⁴ ₋₁₄₁	4.9	3	5.7 ^{+0.7} _{-0.8}	0.95	0.16	0.13
PSZ2 G250.04+24.14	0.411 ± 0.001			29	29	1065 ⁺⁴⁴⁷ ₋₂₈₅		1466 ⁺³⁸⁰ ₋₂₄₁	6.2	3	6.2 ± 0.6	0.94	0.97	0.10
PSZ2 G251.13-78.15	0.306 ± 0.001	+		17	17	801 ⁺⁸⁵² ₋₄₉₅		1188 ⁺²⁰⁵ ₋₁₅₅	4.8	1	4.1 ± 0.6	0.56	0.19	0.26
PSZ2 G272.85+48.79	0.420 ± 0.002			10	9	1462 ⁺³⁸⁹ ₋₂₁₆		1498 ⁺³⁴⁵ ₋₁₇₅	4.8	2	5.3 ^{+0.7} _{-0.8}	0.98	0.61	0.62
PSZ2 G329.48-22.67	0.249 ± 0.001	+		19	16	835 ⁺¹⁷⁹ ₋₁₁₉		746 ⁺¹⁵² ₋₆₄	6.0	3	5.0 ^{+0.7} _{-0.8}	0.99	0.90	0.46
PSZ2 G348.43-25.50	0.265 ± 0.001			21	20	1065 ⁺⁴¹¹ ₋₁₉₈		1160 ⁺²⁷⁷ ₋₁₀₇	7.1	3	6.0 ± 0.6	0.85	0.18	0.02
PSZ2 G352.05-24.01 ^a	0.786 ± 0.026			23	10	–	–	–	4.1	1	6.2 ^{+0.9} _{-1.0}	0.35	0.02	0.03
	0.304 ± 0.022			23	13	–	–	–				0.99	0.94	0.98

^aTwo structures observed, not confirmed as clusters (see text and Figure B2).

PSZ2 G251.13-78.15 was detected by one method with a $S/N \sim 4.8$ (*Planck* reliability of $\sim 90\%$), its redshift distribution has a K-S and a S-W probability of $\sim 60\%$ and $\sim 20\%$, respectively, to be Gaussian, and a $\sim 3\%$ probability of not being a cluster. We consider it as a confirmed cluster, and again notice the larger uncertainty in its confirmation, mass and velocity dispersion estimates. This is a newly spectroscopically confirmed cluster.

PSZ2 G272.85+48.79 was detected by two methods with a $S/N \sim 5$ (*Planck* reliability of $\sim 92\%$). From the combined *Planck* and K-S gaussian probabilities, it has a 90% probability of being a cluster. On the other hand, from the combined *Planck* and K-S uniform probabilities, it has a 5% of probability of not being a cluster. According to our criteria this is at the limit of being confirmed as a cluster of galaxies. However, we assume it is confirmed, also considering that it is more massive than $10^{14} M_{\odot}$ (e.g. Evrard et al. 2008).

For PSZ2 G352.05-24.01, the redshift obtained from the X-ray analysis is $z = 0.79$ (*Planck Collaboration et al. 2013*), but we observe galaxies in a wider redshift range. In fact, we can distinguish two structures at $z \sim 0.8$ and $z \sim 0.3$, shown in blue and green, respectively, in Figure B2. Both redshift distributions have a standard deviation of ~ 0.08 , much wider of what expected for a cluster of galaxies. This target is not a cluster of galaxies, and we have excluded it from the analysis of the velocity dispersion–mass relation in Amodeo et al. (2017).

PSZ2 G085.95+25.23, confirmed at $z = 0.782 \pm 0.010$, is one of the highest redshift confirmed *Planck* clusters.

Newly confirmed clusters are labeled with the sign ”+” in Table 3.

4. SPECTROSCOPIC REDSHIFT CATALOGS

We provide the cluster catalogs as electronic documents, including the following parameters for each cluster galaxy:

1. the galaxy identification number ID
2. the J2000 right ascension R.A., in hours
3. the J2000 declination Decl., in deg
4. the measured spectroscopic redshift SPECZ
5. the error in spectroscopic redshift eSPECZ

An example is shown in Table C2 for PSZ2G053.44-36.25.

5. DISCUSSION

In the context of the optical identification of *Planck* cluster candidates, our sample, although small, is chosen to have a wide range of mass with the aim of obtaining a statistical calibration of the *Planck* SZ mass estimator. In this section, we compare it with previous *Planck* cluster redshift measurements.

Eight of our targets are in the SDSS DR8 redMaPPer cluster catalogs (Wen et al. 2012; Rykoff et al. 2014). Five

of them (PSZ2G108.71-47.75, PSZ2 G186.99+38.65, PSZ2 G216.62+47.00, PSZ2 G056.93-55.08, and PSZ2 G083.29-31.03) have previous spectroscopic redshift measurements in agreement with our values.

Measurements of galaxy redshifts are available in the SDSS DR14 in seven of our fields. A search within two virial radii from the center of each of our clusters finds spectroscopic catalogs for galaxies in the following clusters ($N_{\text{gal, DR14}}$): PSZ2 G053.44-36.25 (15), PSZ2 G056.93-55.08 (3), PSZ2 G081.00-50.93 (8), PSZ2 G083.29-31.03 (32), PSZ2 G108.71-47.75 (3), PSZ2 G186.99+38.65 (24), PSZ2 G216.62+47.00 (19). We included these redshifts and we recalculated the cluster redshifts and velocity dispersions with the same procedure (see Table 3). The redshift estimates do not change, while the uncertainties are smaller. Velocity dispersions are on average within (0.28 ± 0.17) sigma the values obtained with our measurements only, and never above 0.5 sigma. For the other targets, there are not public spectroscopic redshifts for single galaxies to our knowledge.

The *Planck* collaboration has undertaken two important optical follow-up programs to confirm *Planck* cluster candidates and to measure their redshifts. The first is based on observations with the Russian-Turkish 1.5 m telescope ([Planck Collaboration et al. 2015](#)) and provides spectroscopic redshifts for 65 *Planck* clusters. It includes our targets PSZ2 G139.62+24.18, for which they obtain a spectroscopic redshift of 0.268 consistent with our measurement, and PSZ2 G157.43+30.34, for which they find a photometric redshift of 0.45. [Vorobyev et al. \(2016\)](#) report on additional spectroscopic observations of the latter cluster from the 2.2-m Calar Alto Observatory telescope, obtaining $z = 0.403$ with an error of 1%, consistent with our value of $z = 0.402 \pm 0.006$.

The second program, based on observations with telescopes at the Canary Islands Observatories (Gran Telescopio Canarias, Isaac Newton Telescope, William Herschel Telescope, Telescopio Nazionale Galileo, Nordic Optical Telescope, IAC80 telescope), provided 53 cluster spectroscopic redshifts, and is published in [Planck Collaboration et al. \(2016c\)](#). Again it includes our target PSZ2 G139.62+24.18, for which they measure $z=0.266$ from 22 spectroscopically confirmed members, consistent with our value of $z = 0.268 \pm 0.005$ obtained from 20 galaxies.

The *Planck* collaboration has also carried out X-ray validation programs with *XMM-Newton* ([Planck Collaboration et al. 2011a, 2012, 2013](#)), where redshifts z_{Fe} have been obtained from X-ray spectral fitting of the iron emission line. Targets PSZ2 G250.04+24.14 and PSZ2 G272.85+48.79 are analysed in [Planck Collaboration et al. \(2011a\)](#), PSZ2 G235.56+23.29 in [Planck Collaboration et al. \(2012\)](#), and PSZ2 G348.43-25.50 and PLCK G147.32-16.59 in [Planck Collaboration et al. \(2013\)](#). In all cases, *XMM-Newton* finds redshifts consistent with our values. [Planck Collaboration et al. \(2013\)](#) also includes the X-ray analysis of PSZ2 G329.48-22.67. They observe a double projected system at

redshifts 0.24 and 0.46. In our GMOS analysis, we measure $z = 0.249 \pm 0.003$ based on 16 spectroscopic members, with no detections at higher redshift.

Finally, [Planck Collaboration et al. \(2013\)](#) quote a redshift $z_{\text{Fe}} = 0.77$ for PSZ2 G352.05-24.01. The authors give $z_{\text{Fe}} = 0.12, 0.40$ as other possible solutions to the spectral fitting, but these are excluded from the comparison between the X-ray and SZ properties of the source (Y_{X}/Y_{500}). We observe a sparse galaxy distribution, with two (small) peaks with more than five galaxies, one with six galaxies at $z = 0.798 \pm 0.021$ and the other with 11 at $z = 0.334 \pm 0.025$. However, these large dispersions (~ 3500 km/s at $z=0.798$ and ~ 5600 km/s at $z=0.334$) do not confirm clusters of galaxies, and we do not consider this target as a confirmed cluster.

In conclusion, six of our clusters have spectroscopic redshifts from previous optical studies, seven have redshift measurements from X-ray spectral fitting. Their velocity dispersions are published in this paper for the first time. For the remaining seven clusters, spectroscopic redshifts and velocity dispersions are published in this paper for the first time.

6. CONCLUSIONS

This article presents spectroscopic redshifts and velocity dispersions for 20 *Planck* SZ clusters. We spectroscopically confirm 19 clusters with Gemini-North and Gemini-South/GMOS, six of which were spectroscopically confirmed in this paper for the first time. We also confirm and measure the redshift and velocity dispersion of the *Planck* cluster PSZ2 G085.95+25.23 with Keck/LRIS spectroscopy, measuring a mean redshift of $z = 0.782 \pm 0.010$, one of the *Planck*'s highest redshift confirmed clusters. Eighteen of our clusters are included in the last released *Planck* SZ source catalog, PSZ2 ([Planck Collaboration et al. 2016b](#)).

We provide online catalogs for each cluster spectroscopic member redshift (an example is shown in Table C2).

In a companion paper ([Amodeo et al. 2017](#)) we use the cluster galaxy velocity dispersions to measure the *Planck* mass bias, and to constrain the cluster velocity bias.

Based on observations obtained at the Gemini Observatory (Programs GN-2011A-Q-119, GN-2011B-Q-41, and GS-2012A-Q-77; P.I. J.G. Bartlett), which is operated by the Association of Universities for Research in Astronomy, Inc., under a cooperative agreement with the NSF on behalf of the Gemini partnership: the National Science Foundation (United States), the National Research Council (Canada), CONICYT (Chile), Ministerio de Ciencia, Tecnología e Innovación Productiva (Argentina), and Ministério da Ciência, Tecnologia e Inovação (Brazil). Supported by the Gemini Observatory, which is operated by the Association of Universities for Research in Astronomy, Inc., on behalf of the international Gemini partnership of Argentina, Brazil, Canada, Chile, and the United States of America. This material is based upon work supported by AURA through the National Sci-

ence Foundation under AURA Cooperative Agreement AST 0132798 as amended. We are pleased to acknowledge the Palomar Observatory staff for their enthusiastic and excellent support. Part of the data presented herein were obtained at the W. M. Keck Observatory, which is operated as a scientific partnership among the California Institute of Technology, the University of California and the National Aeronautics and Space Administration. The Observatory was made possible by the generous financial support of the W. M. Keck Foundation. The authors wish to recognize and acknowledge the very significant cultural role and reverence that the summit of Maunakea has always had within the indigenous Hawaiian community. We are most fortunate to have the opportunity to conduct observations from this mountain. We thank

the P.I. of the Keck observations, Fiona Harrison, and Mislav Baloković and George Lansbury for participating in the Keck observations. J.G.B. and S.M. acknowledge financial support from the *Institut Universitaire de France (IUF)* as senior members. Part of the work of J.G.B., C.L. and D.S. was carried out at the Jet Propulsion Laboratory, California Institute of Technology, under a contract with NASA. S.M.'s research was supported by an appointment to the NASA Postdoctoral Program at the Jet Propulsion Laboratory, administered by Universities Space Research Association under contract with NASA. We thank the referee for her/his useful comments that helped improve the presentation of this work, and Joanne Cohn for useful discussion.

Facility: Gemini: South, Gemini: Gillet, Hale, Keck:I (LRIS), Planck

REFERENCES

- Allen, S. W., Evrard, A. E., & Mantz, A. B. 2011, *ARA&A*, 49, 409
 Amodeo, S., Mei, S., Stanford, S. A., et al. 2017, *ApJ*, 844, 101
 Beers, T. C., Flynn, K., & Gebhardt, K. 1990, *AJ*, 100, 32
 Birkinshaw, M. 1999, *PhR*, 310, 97
 Bruzual, G., & Charlot, S. 2003, *MNRAS*, 344, 1000
 Carlstrom, J. E., Holder, G. P., & Reese, E. D. 2002, *ARA&A*, 40, 643
 Evrard, A. E., Bialek, J., Busha, M., et al. 2008, *ApJ*, 672, 122
 Fasano, G., & Franceschini, A. 1987, *MNRAS*, 225, 155
 Girardi, M., Biviano, A., Giuricin, G., Mardirossian, F., & Mezzetti, M. 1993, *ApJ*, 404, 38
 Girardi, M., Demarco, R., Rosati, P., & Borgani, S. 2005, *A&A*, 442, 29
 Gladders, M. D., & Yee, H. K. C. 2000, *AJ*, 120, 2148
 Licitra, R., Mei, S., Raichoor, A., Erben, T., & Hildebrandt, H. 2016a, *MNRAS*, 455, 3020
 Licitra, R., Mei, S., Raichoor, A., et al. 2016b, *ApJ*, 829, 44
 Massey, P., & Gronwall, C. 1990, *ApJ*, 358, 344
 Mei, S., Holden, B. P., Blakeslee, J. P., et al. 2009, *ApJ*, 690, 42
 Melin, J.-B., Bartlett, J. G., & Delabrouille, J. 2006, *A&A*, 459, 341
 Mroczkowski, T., Kovács, A., Bulbul, E., et al. 2015, *ApJL*, 808, L6
 Oke, J. B., Cohen, J. G., Carr, M., et al. 1995, *PASP*, 107, 375
 Planck Collaboration, Aghanim, N., Arnaud, M., et al. 2011a, *A&A*, 536, A9
 Planck Collaboration, Ade, P. A. R., Aghanim, N., et al. 2011b, *A&A*, 536, A8
 Planck Collaboration, Aghanim, N., Arnaud, M., et al. 2012, *A&A*, 543, A102
 Planck Collaboration, Ade, P. A. R., Aghanim, N., et al. 2013, *A&A*, 550, A130
 —. 2014, *A&A*, 571, A29
 —. 2015, *A&A*, 582, A29
 —. 2016a, *A&A*, 594, A13
 —. 2016b, *A&A*, 594, A27
 —. 2016c, *A&A*, 586, A139
 Rykoff, E. S., Rozo, E., Busha, M. T., et al. 2014, *ApJ*, 785, 104
 Shapiro, S. S., & Wilk, M. B. 1965, *Biometrika*, 52, 591
 Sunyaev, R. A., & Zeldovich, Y. B. 1970, *Ap&SS*, 7, 3
 Truemper, J. 1993, *Science*, 260, 1769
 Valdes, F. G., Campusano, L. E., Velasquez, J. D., & Stetson, P. B. 1995, *PASP*, 107, 1119
 van Weeren, R. J., Intema, H. T., Lal, D. V., et al. 2014, *ApJL*, 781, L32
 Vorobyev, V. S., Burenin, R. A., Bikmaev, I. F., et al. 2016, *Astronomy Letters*, 42, 63
 Wen, Z. L., Han, J. L., & Liu, F. S. 2012, *ApJS*, 199, 34
 White, M., Cohn, J. D., & Smit, R. 2010, *MNRAS*, 408, 1818
 York, D. G., Adelman, J., Anderson, Jr., J. E., et al. 2000, *AJ*, 120, 1579

APPENDIX

A. *Planck* CLUSTERS OBSERVED WITH THE PALOMAR TELESCOPE

Table A1. *Planck* clusters observed with the Palomar telescope. Clusters are named after their PSZ2 or PSZ1 ID, when available. When it is not available, we use the prefix 'PLCK' followed by a notation in Galactic coordinates similar to that used in the PSZ2 paper.

Name	R.A. (deg)	Decl. (deg)	Filter	Instrument	Run
PSZ2 G019.12+31.23	249.1420	3.1528	g', i'	LFC	2011A
PLCK G024.20+58.78	225.5920	18.6586	g', i'	LFC	2011A
PLCK G030.89+42.25	243.3310	16.4481	g', i', r'	LFC	2011A
PSZ2 G066.41+27.03	269.2120	40.1156	g', i', r'	LFC	2011A
PLCK G071.59-63.16	351.9458	-8.9647	i'	LFC	2012B
PSZ2 G074.08-54.68	347.0917	-1.9106	i'	LFC	2012B
PSZ2 G078.67+20.06	282.9920	49.0257	g', i'	LFC	2011A
PSZ2 G082.31-67.00	357.9500	-8.9647	i'	LFC	2012B
PSZ2 G086.93+53.18	228.4790	52.7775	g', i'	LFC	2011A
PLCK G087.67+23.00	282.3250	57.8956	g', i'	LFC	2011A
PSZ2 G091.83+26.11	277.8080	62.2317	i', r'	LFC	2011A
PSZ2 G094.56+51.03	227.0960	57.8706	g', i', r'	LFC	2011A
PLCK G096.88+24.22	284.0750	66.3819	g', i'	LFC	2011A
PSZ2 G107.83-45.45	1.8753	16.1423	g', r', J, K	LFC, WIRC	2010B
PSZ1 G108.52+32.30	256.9920	76.4697	g', r', i'	LFC	2011A
PLCK G109.35+64.36	202.3080	51.7589	g', i'	LFC	2011A
PLCK G113.07-74.37	10.1610	-11.7062	r', J, K	LFC, WIRC	2010B
PLCK G113.66+70.59	197.2970	46.2171	g', i'	LFC	2011A
PLCK G114.92-20.06	2.6792	42.1783	i'	LFC	2012B
PLCK G116.80-25.18	5.8708	37.3600	i'	LFC	2012B
PLCK G117.14-26.47	6.4417	36.1117	i'	LFC	2012B
PSZ1 G121.09+57.02	194.8400	60.0897	g', i', r'	LFC	2011A
PSZ1 G129.07-24.12	20.0000	38.4531	g', i'	LFC	2011B
PSZ2 G134.26-44.28	21.3542	17.8808	g', i'	LFC	2011B
PSZ2 G138.11+42.06	157.0542	70.6081	g', i', r', J, K	LFC, WIRC	2010B, 2011A, 2011B
PSZ2 G139.62+24.18	95.4912	74.7042	g', i', r', J, K	LFC, WIRC	2010B, 2011A
PLCK G142.35+17.59	78.8752	69.7009	g', J	LFC, WIRC	2010B, 2011A
PLCK G147.32-16.59 ^a	44.1000	40.2911	g', i', r'	LFC	2011B
PSZ2 G157.43+30.34	117.2208	59.6944	g', i', r', J, K	LFC, WIRC	2010B, 2011A, 2011B
PLCK G159.41-62.64	28.7625	-4.3600	g'	LFC	2011B
PSZ2 G171.98-40.66	48.2307	8.3805	g', r', K	LFC, WIRC	2010B
PSZ2 G172.93+21.34	106.8920	44.3050	r'	LFC	2011A
PLCK G183.33-36.69	57.2936	4.5974	g', J, K	LFC, WIRC	2010B
PSZ2 G183.30+34.98	127.4042	38.4325	g', i'	LFC	2011B
PLCK G184.34+29.07	120.3380	36.4269	g', i'	LFC	2011A
PSZ2 G193.31-46.13	53.9592	-6.9853	g', r', J, K	LFC, WIRC	2010B
PSZ2 G193.63+54.85	152.5750	32.8472	i'	LFC	2011B
PSZ2 G194.68-49.76	51.3625	-9.6181	i'	LFC	2012B
PSZ2 G196.65-45.51	55.7583	-8.7039	i'	LFC	2012B
PLCK G196.72+23.27	118.2330	24.2689	g', i'	LFC	2011A
PLCK G198.13-24.68	74.3315	0.9310	r', J, K	LFC, WIRC	2010B
PSZ2 G198.90+18.16	113.4333	20.3083	g', i'	LFC	2011B
PLCK G201.89+32.14	128.5292	22.7656	g', i'	LFC	2011B
PSZ1 G203.88+62.50	161.7580	27.9606	i'	LFC	2011A
PSZ2 G204.24+14.51	112.1375	14.1283	g', i'	LFC	2012B
PSZ2 G205.90+73.76	174.5833	27.9186	g', i'	LFC	2011B
PLCK G211.37+49.36	148.5583	21.2128	g', i'	LFC	2011B
PSZ2 G212.44+63.19	163.2292	24.2128	g', i'	LFC	2011B
PLCK G214.57+36.96	137.1950	14.7084	r'	LFC	2011A
PLCK G219.13+52.94	153.8580	17.8178	g', i', r', J, K	LFC, WIRC	2010B, 2011A
PSZ1 G223.80+58.50	160.3292	17.5111	g', i'	LFC	2011B
PLCK G247.33+63.53	170.8870	10.6117	g', i'	LFC	2011A
PSZ1 G263.75+53.85	170.9875	-2.2161	g', i'	LFC	2011B

^aTarget PLCK G147.32-16.59 is confirmed in the *XMM-Newton* cluster validation (Planck Collaboration et al. 2013), but it is not included in the two *Planck* catalogs of SZ sources released so far.

B. REDSHIFT HISTOGRAMS, OPTICAL IMAGES AND SZ MAPS

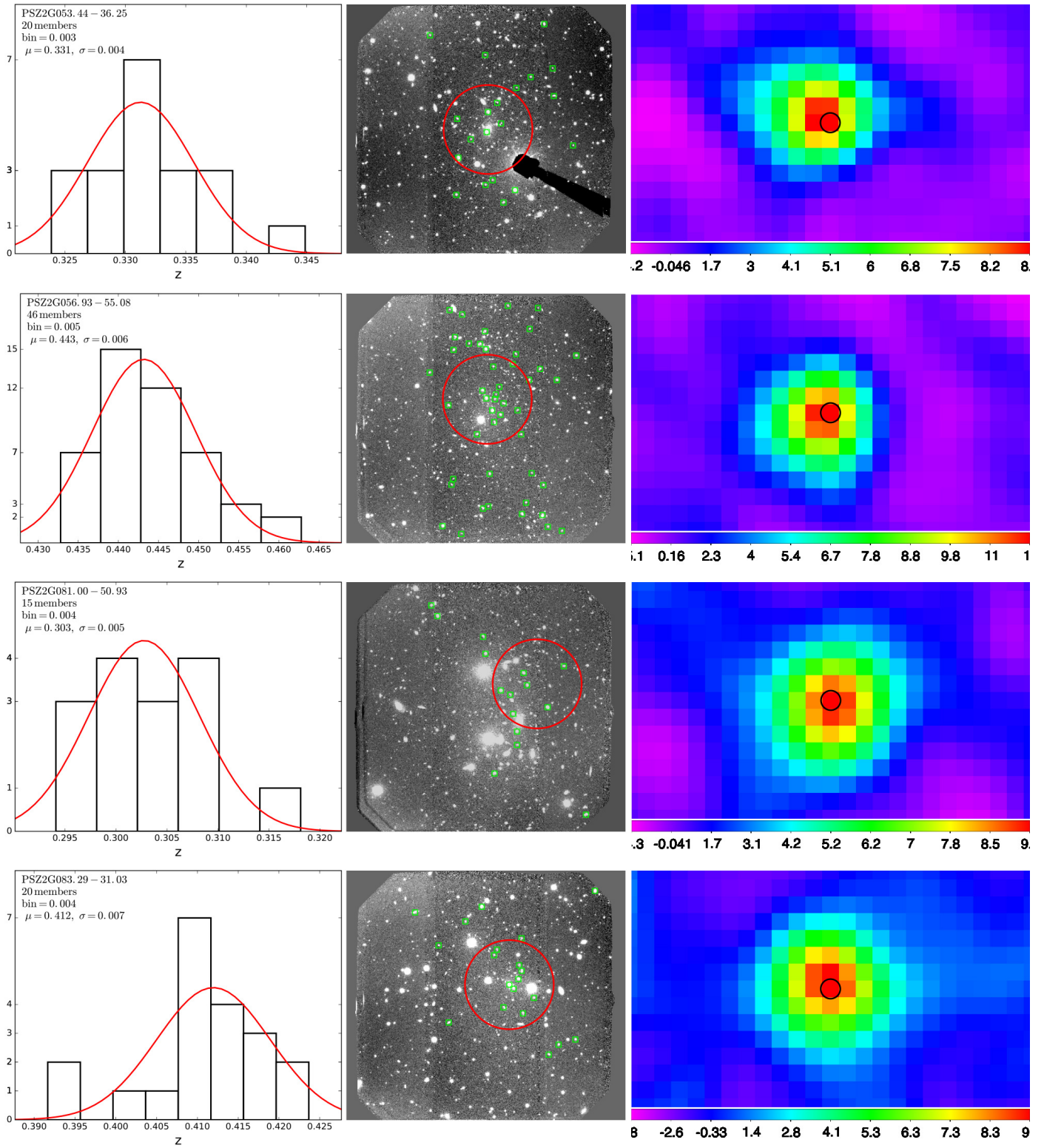
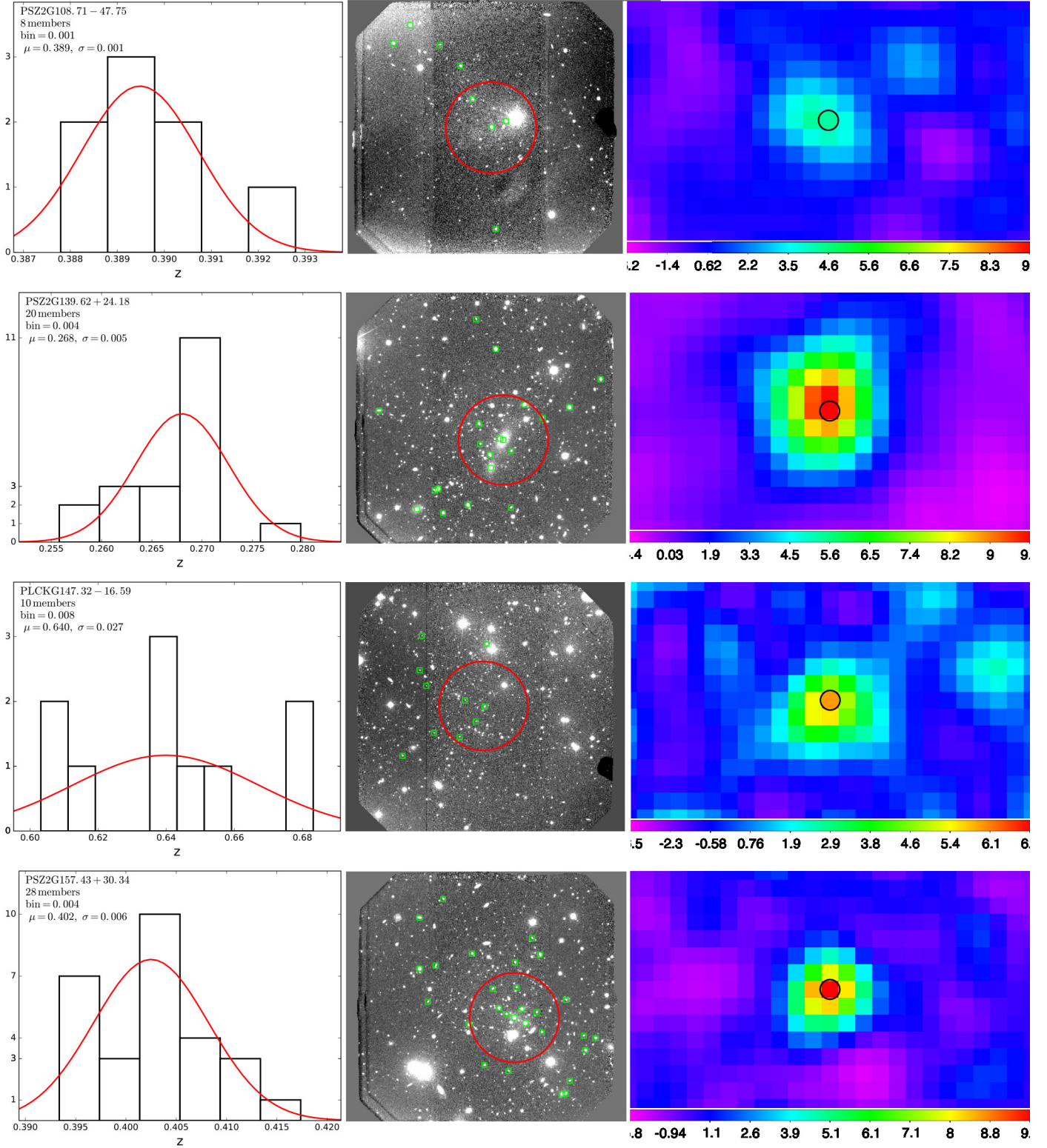


Figure B1 continued



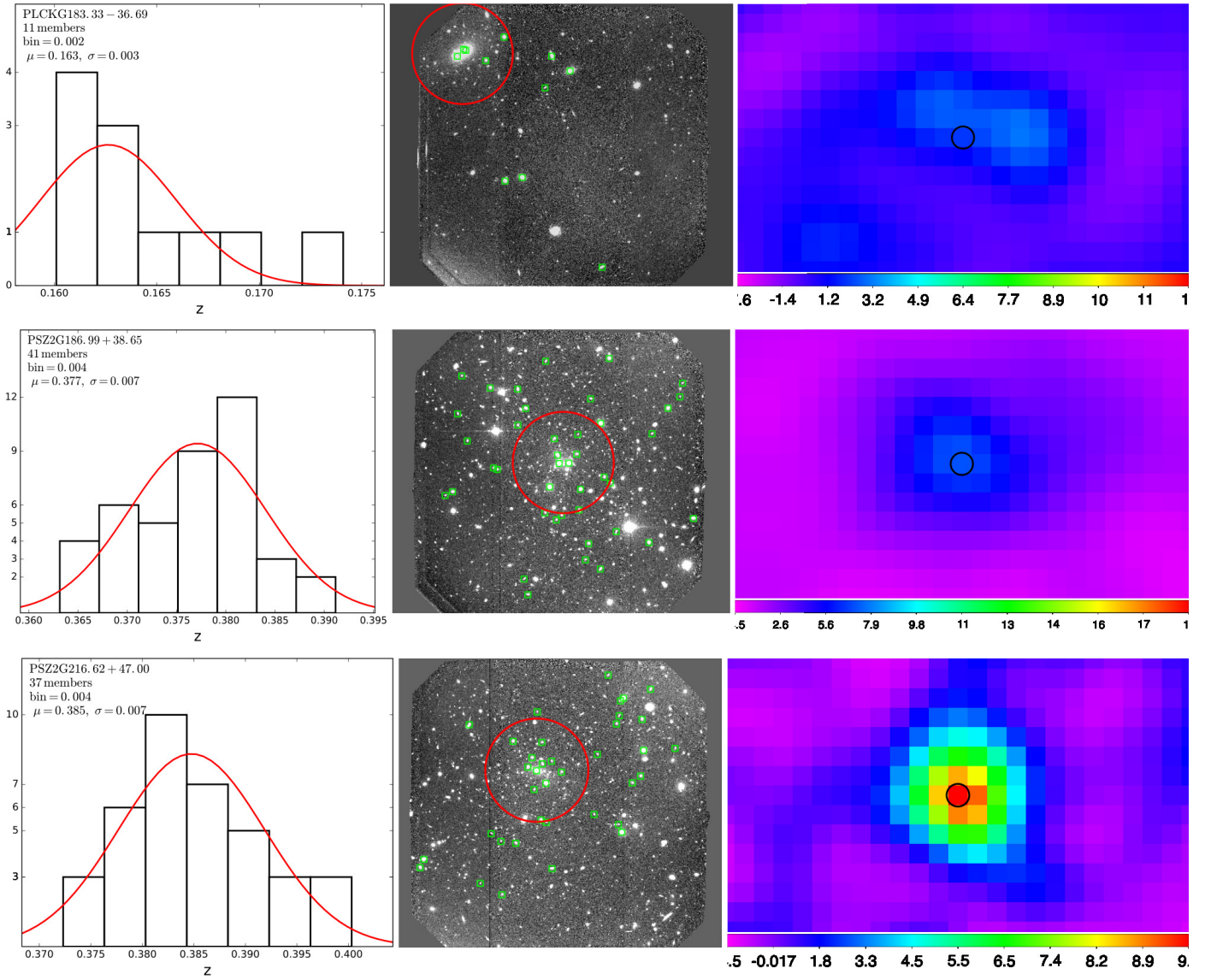
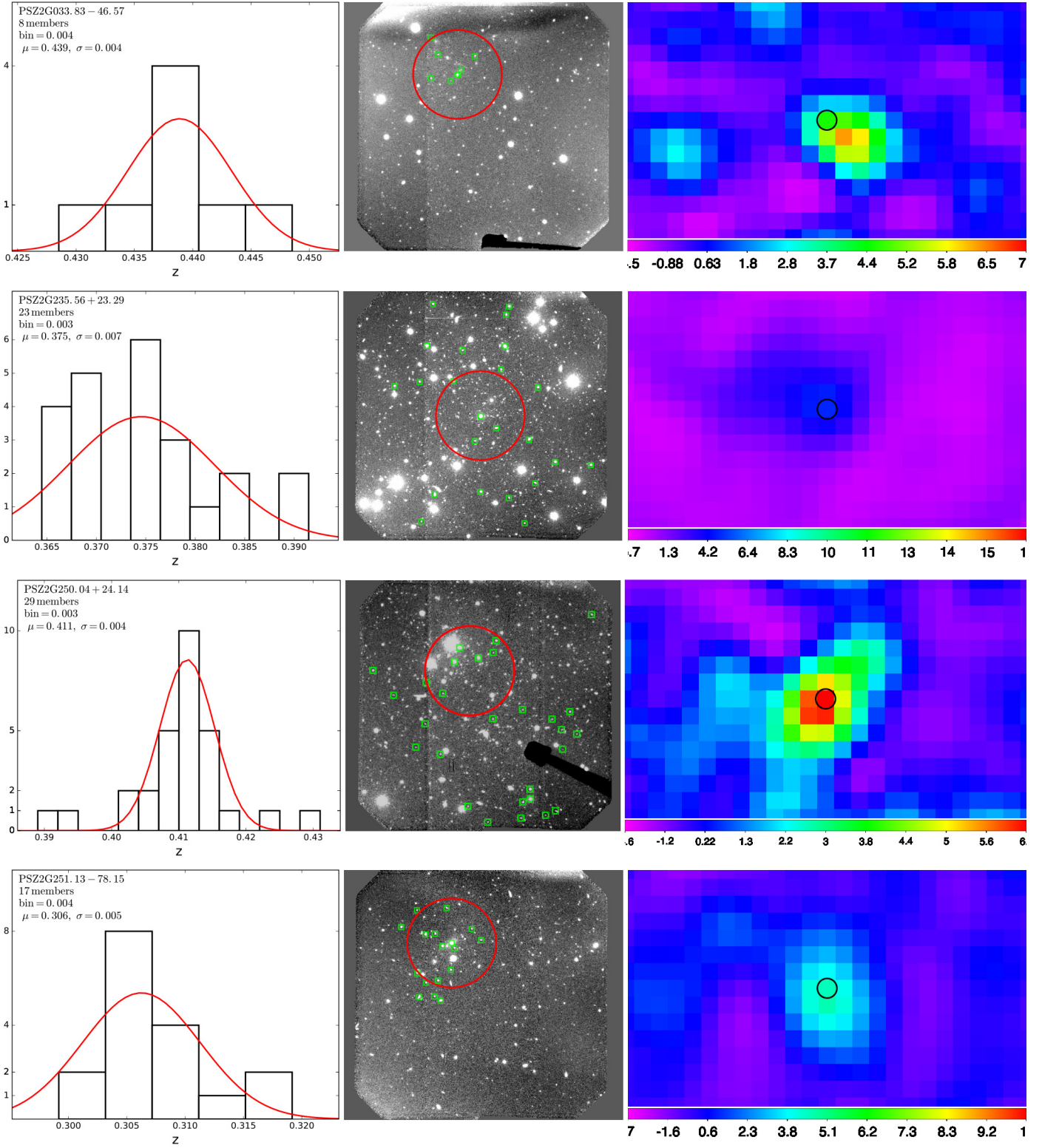


Figure B1. Redshift histograms (left), optical images (middle) and SZ maps in signal-to-noise units (right) of clusters in the Northern sample. The red curve in the histograms is a Gaussian fit with mean (μ) and standard deviation (σ) indicated in the legends, calculated for the redshift distribution using the biweight method. We also indicate the number of members in each cluster and the size of the redshift bins. The red (black) circles in the images enclose a circle of radius 1 arcmin around the optical (SZ) center of the clusters, while the confirmed member galaxies are shown by green squares.



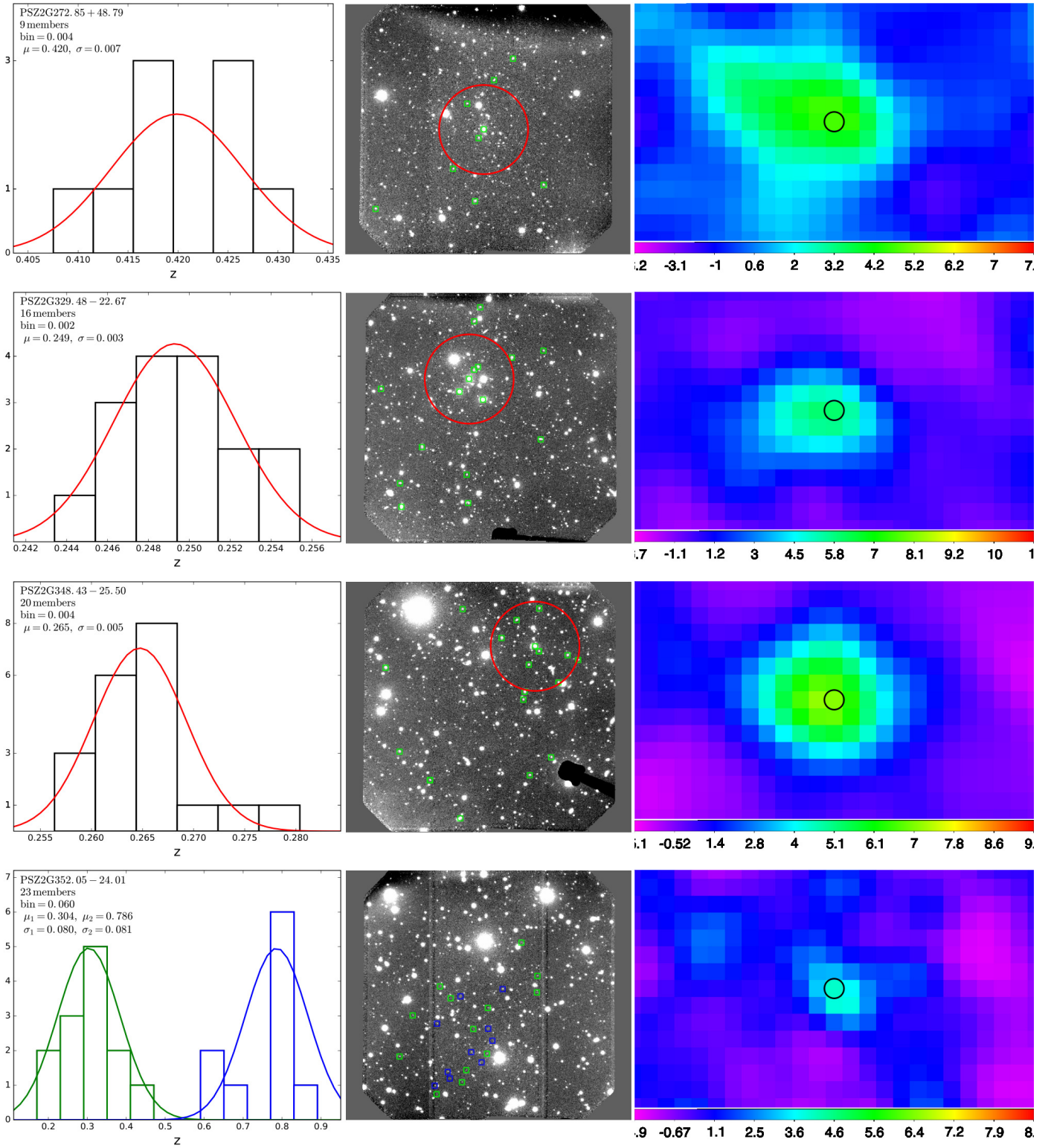


Figure B2. Redshift histograms, optical images and SZ maps of clusters in the Southern sample. Symbols are the same as for Figure B1. For PSZ2 G352.05-24.01, we know only the coordinates of the X-ray center, marked with a red cross.

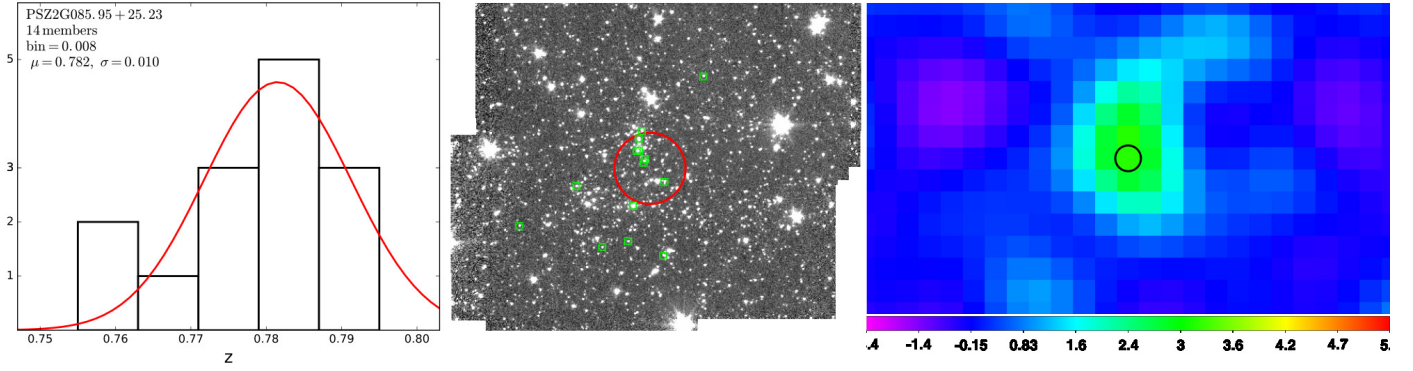


Figure B3. Redshift histogram, IRAC image and SZ map of PSZ2 G085.95+25.23 observed at the Keck telescope. Symbols are the same as for Figure B1.

C. SPECTROSCOPIC REDSHIFT CATALOG OF PSZ2 G053.44-36.25 MEMBER GALAXIES

Table C2. Catalog of galaxies detected for cluster PSZ2 G053.44-36.25. The full spectroscopic catalog is available in the online version of the journal.

ID	R.A. (deg)	Decl. (deg)	SPECZ	eSPECZ
1	21.58816	-1.08456	0.3306	0.0002
2	21.58506	-1.06186	0.3324	0.0001
3	21.58748	-1.05329	0.3363	0.0001
4	21.58530	-1.08879	0.3304	0.0003
5	21.58638	-1.05156	0.3361	0.0003
6	21.58564	-1.06893	0.3258	0.0002
7	21.58671	-1.05585	0.3359	0.0001
8	21.58600	-1.06488	0.3301	0.0002
9	21.58632	-1.02193	0.3344	0.0003
10	21.58714	-1.04561	0.3277	0.0002
11	21.58603	-1.02659	0.3345	0.0002
12	21.58648	-1.05931	0.3239	0.0002
13	21.58509	-1.07221	0.3316	0.0002
14	21.58678	-1.07722	0.3322	0.0003
15	21.58659	-1.03027	0.3250	0.0003
16	21.58745	-1.03873	0.3335	0.0001
17	21.58458	-1.04332	0.3307	0.0002
18	21.58804	-1.03449	0.3891	0.0006
19	21.58677	-1.02851	0.3424	0.0004
20	21.58674	-1.04831	0.3276	0.0002